Analysis of Quantum Yields for the Photolysis of Formaldehyde at $\lambda > 310$ nm†

J. Troe‡

Institut für Physikalische Chemie, Universität Göttingen, Tammannstrasse 6, D-37077 Göttingen, Germany

Received: October 20, 2006; In Final Form: December 14, 2006

Experimental quantum yields of the photolysis of formaldehyde at $\lambda > 310$ nm are combined with absolute and relative rate calculations for the molecular elimination $H_2CO \rightarrow H_2 + CO$ (1), the bond fission $H_2CO \rightarrow H + HCO$ (2), and the intramolecular hydrogen abstraction $H_2CO \rightarrow H \cdots HCO \rightarrow H_2 + CO$ (3) taking place in the electronic ground state. Temperature and pressure dependencies of the quantum yields are analyzed with the goal to achieve consistency between experiment and modeling. Two wavelength ranges with considerably different properties are considered: 340−360 nm, where channel 1 competes with collisional deactivation of excited molecules, and 310−340 nm, which is dominated by the competition between the formation of radical and molecular products. The close relation between photolysis and pyrolysis of formaldehyde, such as analyzed for the pyrolysis in the companion paper, is documented and an internally consistent treatment of the two reaction systems is provided. The quantum yields are modeled and represented in analytical form such that values outside the available experimental range can be predicted to some extent.

I. Introduction

Formaldehyde is a common intermediate of the oxidation of hydrocarbons. It plays an important role in atmospheric photochemistry[1] as well as in combustion kinetics.[2] As a consequence, a large number of experimental studies have been devoted to its reactions (see, e.g., the recent evaluations of rate data in refs 3−5). Among these studies, photolysis and pyrolysis have received particular attention. It is known that the two processes are intimately related. In spite of this fact, the two reaction systems have only rarely been interpreted in an internally consistent way. A first attempt was made in ref 6 to rationalize rate coefficients of the thermal dissociation on the basis of information derived from photodissociation studies. A refined version of this analysis[7] has accounted for finer details and newer experimental as well as theoretical results. This article provides the complementary analysis of photolysis quantum yields taking advantage of information derived from pyrolysis experiments. References 6 and 7 and the present work, therefore, should be understood as belonging together and illustrating two complementary aspects of the same reaction dynamics. The link between photolysis and pyrolysis in this way becomes particularly evident.

Formaldehyde is known to dissociate into the radical products H + HCO and the molecular products H_2 + CO. The almost thermoneutral elimination process with molecular products in our work is termed "channel 1". Its barrier is known to be large

$$H_2CO \rightarrow H_2 + CO \qquad (1)$$

and only slightly smaller than the threshold energy for bond-breaking, which is termed "channel 2" and which gives rise to

$$H_2CO \rightarrow H + HCO \qquad (2)$$

the multichannel character of the thermal dissociation reaction. One now knows that there is an additional "channel 3" that also leads to molecular products via intramolecular hydrogen abstraction, symbolized by

$$H_2CO \rightarrow H \cdots HCO \rightarrow H_2 + CO \qquad (3)$$

and which opens up at the same threshold energy as channel 2. All three channels have been shown to contribute to the thermal dissociation of formaldehyde[6] but it has to be investigated to what extent channels 1 and 3, at energies above the threshold for channels 2 and 3, need to be separated for rate calculations. Because there is a fast internal conversion H_2CO (S_1) → H_2CO (S_0*) after photoexcitation of formaldehyde in the near UV (see, e.g., the review in ref 8), all channels also contribute to the photolysis. Again the question arises to what extent channels 1 and 3 need to be separated. In addition to channels 1−3, dissociation from the lowest triplet state H_2CO (T_1)

$$H_2CO(T_1) \rightarrow H + HCO \qquad (4)$$

also participates in the photolysis[9−12] because the triplet is accessible by intersystem crossing from $H_2CO(S_1)$. The quantitative contribution of this channel to photolysis also needs to be considered. The present article analyzes and models the properties of the photolysis quantum yields of formaldehyde at $\lambda > 310$ nm, i.e., the wavelength, temperature, and pressure dependences of the yields for molecular and radical products. These quantities are of importance in atmospheric chemistry and they have been discussed and represented, e.g., in refs 4, 5, and 13. The present work goes beyond these evaluations by linking experimental results to theoretical modeling.

Figure 1 illustrates experimental quantum yields for radical products from representative studies[14−17] and from the recommendation of ref 4, which was based on these studies and similar earlier work. Figure 2 gives quantum yields for molecular products from refs 14 and 15 (data for room temperature and 1 bar of air) together with the corresponding interpolated curve from ref 4. Molecular products are formed at wavelengths up to about 360 nm whereas radical products are found only up to about 340 nm. As the threshold energy for radical formation is

† Part of the special issue "James A. Miller Festschrift".

‡ E-mail: shoff@gwdg.de.

10.1021/jp066886w CCC: $37.00
Published on Web 02/01/2007

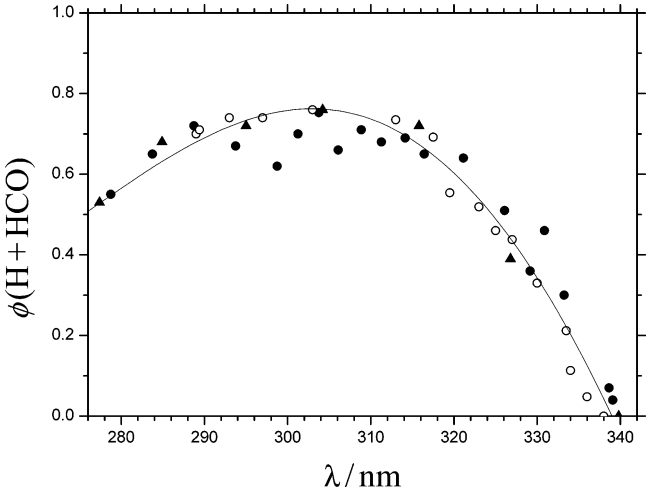

Figure 1. Quantum yields of formaldehyde photolysis to radical products at $T = 300$ K and in 760 Torr of air: experiments from refs 14 and 15 (▲), 16 (○), 17 (●) and the data evaluation from ref 4 (solid line).

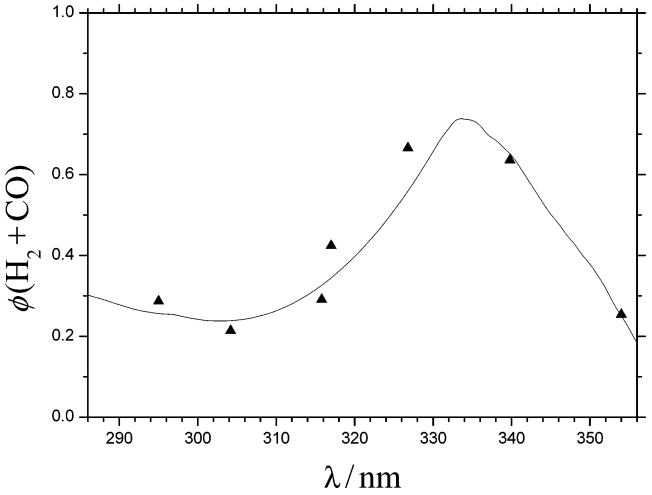

Figure 2. Quantum yields of formaldehyde photolysis to molecular products at $T = 300$ K and in 760 Torr of air: experiments from refs 14 and 15 (▲) and the corresponding data evaluation from ref 4 (solid line).

well-known[18,19] to correspond to $\lambda = 329.7$ nm, radical formation in the range 330−340 nm must also involve thermal excitation of formaldehyde. The barrier for formation of molecular products is less certain,[6,7,20] corresponding to about $\lambda \approx 350$ nm; formation of molecular products in the range 350−360 nm is attributed to tunneling through the elimination barrier (it can be shown that there is not much influence of thermal excitation in this case; see below). Radical formation via the $S_1 \rightarrow T_1$ pathway opens up at wavelengths around 310 nm,[12] but there are also tunneling contributions from this channel at longer wavelengths. The present work focuses on the properties of the quantum yields in two ranges: (i) 340−360 nm where the formation of molecular products is dominated by channel 1 and where the competition between this channel and collisional deactivation determines the quantum yields and (ii) 310−340 nm where radical and molecular products are formed and the effects of the "roaming atom" mechanism[21] are imaged by the quantum yields.[6] The competition among channels 1−4 at wavelengths smaller than 310 nm is not further discussed in the present work.

With the recent confirmation[12,21−26] of the existence of the intramolecular hydrogen abstraction channel 3, earlier inconsistencies between experimental and theoretical results on pyrolysis and photolysis finally could be resolved. Modeling[27−29] of specific rate constants $k(E,J)$ for channel 1 by RRKM theory including tunneling and for channel 2 by a simplified SACM (statistical adiabatic channel model) treatment[28] suggested that the rate of channel 2 markedly exceeds that of channel 1 as soon as both channels are energetically open. As a consequence, without channel 3 there should have been[30] only little formation of molecular products at wavelengths shorter than the threshold for channel 2; this was not observed experimentally.[14−16] Even if the simplified SACM treatment, which was made before an ab initio potential was available, may require a revision today, the conclusions drawn about an inconsistency of the results without considering channel 3 remain valid. More direct evidence for the existence of channel 3 was found by analyzing product distributions in studies of the photodissociation dynamics.[31] The recent investigations all confirmed the earlier suggestions of the additional channel and classical trajectory calculations[22,26] on a detailed ab initio potential energy surface[32] supported the conclusions. The quantum yields for photolysis at $\lambda < 340$ nm as well as the branching ratios of the pyrolysis, therefore, should all be influenced by the presence of channel 3 and earlier interpretations without account for this channel have become obsolete. Looking into finer details, a comparison of the calculated energy-dependent branching ratios for radical and molecular products with experimental quantum yields, for wavelengths shorter than 330 nm, indicated some uncertainties[6] that will be further explored in the present work. At the same time, minor differences to pyrolysis results[7] will be discussed.

II. Quantum Yields for 340−360 nm

Excitation of formaldehyde at the long-wavelength end of the absorption spectrum[4,5] through internal conversion $S_1 \rightarrow S_0^*$ leads to vibrationally highly excited electronic ground state molecules S_0^* that either eliminate $H_2 + CO$ via channel 1 or are collisionally stabilized. The elimination process can take place at energies E above the threshold energy $E_{0,1}$ or, with the help of tunneling, at $E < E_{0,1}$. Modeling the specific rate constant $k_1(E,J)$ of this channel, therefore, crucially depends on the precise values of the height and the imaginary frequency in the tunneling direction of the barrier. There has been some discussion about the value of $E_{0,1}$. It was located at 79.2(±0.8) kcal mol^{-1} on the basis of an RRKM analysis of measured specific rate constants and experimental densities of states in ref 33. Ab initio calculations from ref 20, combined with a reanalysis of the experiments from ref 33 questioning the significance of the measured densities of states, instead suggested the higher value of 81.9(±0.3) kcal mol^{-1}. The analysis of the thermal dissociation rate constants in ref 7 gave a value of 81.7(±0.5) kcal mol^{-1} in good agreement with the higher value. In the present analysis, $E_{0,1}$ is varied over the range 79−83 kcal mol^{-1} and the influence of $E_{0,1}$ on the modeled quantum yields is discussed. Again a high value of $E_{0,1}$ is confirmed and used throughout the present article. The imaginary barrier frequency was taken as 1840i cm^{-1} from ref 32. As the transition state structure is not too different from the structure of the molecule,[32,34] the effect of rotations on $E_{0,1}$ is easily estimated and approximated by $E_{0,1}(J) \approx E_{0,1}(J=0) + B^{\neq}hcJ(J+1)$ with $B^{\neq} \approx 1.11$ cm^{-1} derived from ref 30 (E in this article always includes vibrational and rotational energy, with the zero level put at the rovibrational ground state of S_0). Because the corresponding rotational energy is given by $E_{rot}(J) \approx BhcJ(J+1)$ with $B \approx 1.21$ cm^{-1}, thermal rotational excitation of formaldehyde practically does not help to overcome the barrier of channel 1.

The electric dipole-forbidden 0−0 transition for the $S_0 \rightarrow S_1$ transition is located at 355.59 nm (80.6 kcal/mol), and the first allowed transition occurs near 353.19 nm (80.9 kcal mol^{-1}); see ref 35. Excitation near $\lambda = 353$ nm followed by internal conversion, therefore, leads to S_0* molecules that can react only by tunneling. Even if molecules are produced in S_0* at energies slightly above $E_{0,1}$, energies in the tunneling range are reached by collisional deactivation. Tunneling, therefore, is of central importance for explaining quantum yields at $\lambda \geq 340$ nm.

In the following, specific rate constants $k_1(E,J=0)$ for formaldehyde dissociation on channel 1, in the tunneling range and above $E_{0,1}$, are calculated by statistical unimolecular rate theory such as described before.[27−29,36−39] The expression

$$k_1(E,J) = W_1(E,J)/h\rho(E,J) \qquad (5)$$

is used where the density of states $\rho(E,J)$ is calculated including anharmonicity contributions such as estimated in the Appendix of ref 6 (i.e., $F_{anh}(E,J) \approx 1 + 0.89\{(E + E_z)/[E_{0,1}(J) + E_z]\}^3$ with $E_z/hc = 5873$ cm^{-1}) and using the ground state frequencies 1180, 1258, 1529, 1764, 2931, and 2997 cm^{-1} from the ab initio calculations of ref 32. These frequencies are used together with the corresponding activated complex frequencies 744, 833, 1246, 1835 and 3127 cm^{-1} from ref 32 such that $W_1(E,J)$ and $\rho(E,J)$ are calculated in a consistent way. Barrier tunneling and reflection contributions are accounted for by using the expression

$$W_1(E,J) = \int_0^E p(x,J)\rho^{\neq}(E - x,J)\,dx \qquad (6)$$

see, e.g., ref 27, where $\rho^{\neq}(E-x,J)$ denotes the density of states of the activated complex at the energy $E - x$ and $p(x,J)$ is the tunneling probability. Without tunneling, one would have $p(x,J) = 1$ at $x \geq E_{0,1}(J)$ and $p(x,J) = 0$ for $x < E_{0,1}(J)$. In the presence of barrier tunneling and reflection, $p(x,J)$ is expressed by the relation for a parabolic barrier,

$$p(E,J) = \frac{1}{2}\{1 + \tanh[(D/2)(E/E_{0,1}(J) - 1)]\} \qquad (7)$$

where the parameter D is given by $D = 2\pi E_{0,1}/|h\nu^*|$ with the imaginary barrier frequency ν^* and the barrier height $E_{0,1}$. The treatment in ref 27 was done with a value of $D = 94.38$. Using the newer values for $E_{0,1}$ and ν^*, the present work employs $D = 104.4$ (for $E_{0,1} = 81.9$ kcal mol^{-1}) or 104.8 (for $E_{0,1} = 82.2$ kcal mol^{-1}). Replacing the parabolic barrier by an Eckart barrier only negligibly changes the results. The calculation is straightforward and leads to the results for $k_1(E,J=0)$ illustrated in Figure 3. As mentioned above, the curves for $k_1(E,J)$ relative to $k_1(E,J=0)$ are simply shifted along the energy scale by the amount $B^{\neq}hcJ(J+1)$. One recognizes a change of the slopes of the curves near $E = E_{0,1}(J)$. It should be mentioned that the present results for $W_1(E,J=0)$ agree with the cumulative reaction probabilities from ref 39 calculated on the ab initio potential from ref 38.

In the following, we investigate whether the experimental pressure, temperature, and wavelength dependences of the quantum yields from refs 14 and 15 for molecular products, measured at 339 and 353 nm and 220 and 300 K, can be reconciled with simple kinetic models based on the derived $k_1(E,J)$. First, it is assumed that, for the considered conditions, practically all molecules excited to S_1 reach S_0* and do not disappear from S_1 by fluorescence. The observed fluorescence lifetimes[40] support this assumption. Second, it is assumed that only channel 1 contributes here and that the specific constants $k_1(E,J)$ from statistical unimolecular rate theory are realistic.

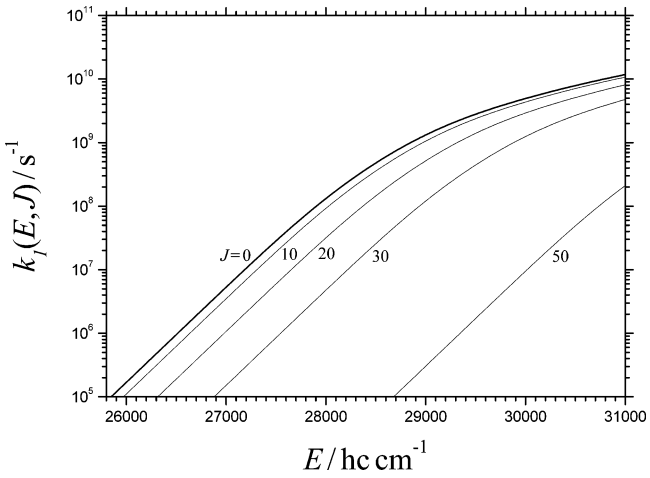

Figure 3. Specific rate constants $k_1(E,J)$ for formaldehyde dissociation on the molecular elimination channel 1 (see text). The used threshold energy $E_{0,1}(J=0)/hc = 28\,640$ cm^{-1} separates the tunneling region from over-barrier reaction.

Finally, it is assumed that S_0* molecules are stabilized in sequences of collisions. One may simulate the latter process in two ways, with a simple stepladder model and, in a more elaborate way, with a master equation. In the stepladder model,[41] each collision removes an amount of $\langle\Delta E\rangle$ from the molecule where $\langle\Delta E\rangle$ denotes the average total energy transferred per collision. This model accounts for microscopic reversibility by combining up and down steps into single steps characterizing total energy transfer. The employed step sizes for up and down transitions here are linked by microscopic reversibility such that $\langle\Delta E\rangle$ intrinsically includes this effect. Collision frequencies Z are represented by Lennard-Jones collision frequencies Z_{LJ}. The fraction of collisionally stabilized molecules, corresponding to $1 - \phi_1$ (ϕ_1 = quantum yield for photolysis on channel 1), in this simple model then follows as

$$1 - \phi_1 = \prod_{i=1}^{\infty}(Z_{LJ}[M]/\{Z_{LJ}[M] + k_1(E - (i-1)|\langle\Delta E\rangle|)\}) \qquad (8)$$

where [M] is the bath gas concentration. With an increasing number of steps i, the factors on the right-hand side of eq 8 approach unity because $k_1(E)$ strongly decreases with decreasing energy E. It was shown in ref 41 that the simple stepladder model gives results that agree with the solutions of a master equation treatment under the condition that $k_1(E)$ is not too steep a function of energy in comparison to the size of $\langle\Delta E\rangle$. If the latter condition is not fulfilled, differences between the two approaches arise.[41,42] In the present situation, this behavior is also observed and is illustrated below. We present this comparison because single-step collision models, up and down step models, and master equation treatments are used alternatively and their comparison appears to be of general interest.

The master equation (neglecting the J dependence) is formulated in the usual way by

$$\frac{dn(E,t)}{dt} = -\{Z_{LJ}[M] + k_1(E)\}n(E,t) + Z_{LJ}[M]\int_0^{\infty} P(E,E')\,n(E',t)\,dE' \qquad (9)$$

where $n(E,t)$ is the population of states at energy E and time t that, at $t = 0$, is normalized to unity. $P(E,E')$ denotes the probability for collisional energy transfer from energy E' to

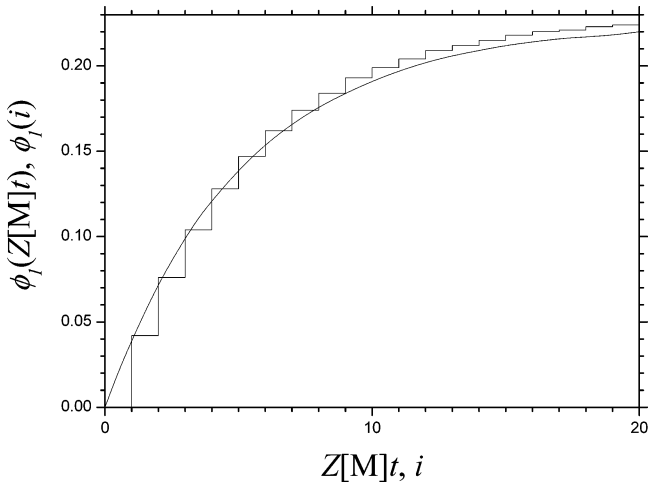

Figure 4. Time-dependent quantum yields of formaldehyde photolysis on the molecular elimination channel 1 after *i* collisions in the stepladder model (with $-\langle\Delta E\rangle/hc = 60$ cm^{-1}, steps) and after Z[M]t collisions in the master equation modeling (with $-\langle\Delta E\rangle/hc = 110$ cm^{-1}, smooth curve). See text. Conditions: $\lambda = 353$ nm, $T = 300$ K, 760 Torr of air, $E_{0,1}(J{=}0)/hc = 28\,640$ cm^{-1}.

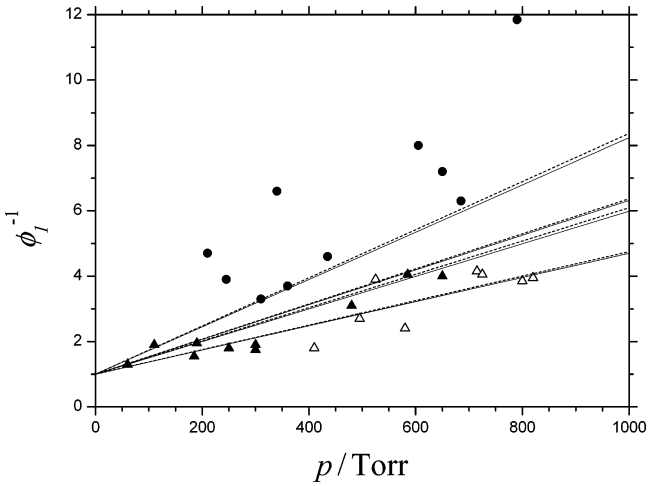

Figure 5. Stern−Volmer plot for formaldehyde photolysis on the molecular elimination channel 1: experimental points for 300 K from ref 14 (△) and 15 (▲) and for 220 K from ref 15 (●). Modeling with $E_{0,1} = 81.9$ kcal mol^{-1} (full lines) and 82.2 kcal mol^{-1} (dashed lines). Lines from bottom to top with (T/K), $E_{0,1}$/kcal mol^{-1}, $-\langle\Delta E\rangle/hc$ cm^{-1}) = (300, 81.9, 80), (300, 82.2, 50), (300, 81.9, 120), (300, 82.2, 80), (220, 81.9, 80), (220, 82.2, 50), (220, 81.9, 120), and (220, 82.2, 80) respectively.

energy E, which in the present work is modeled by a simple exponential collision model[43] with average energies α for down transfer, average energies $\beta \approx \alpha kT/(\alpha + kT)$ for up transfer, and $\langle\Delta E\rangle = \beta - \alpha$. The relation between α and β is a consequence of microscopic reversibility. The integral

$$1 - \phi_1(t) = \int_0^\infty n(E,t)\,\mathrm{d}E \qquad (10)$$

defines a time-dependent quantum yield for collisional stabilization which at $Z_{LJ}[M]t = 1, 2, 3, \ldots$ can be compared with the results from the stepladder model of eq 8 for $i = 1, 2, 3, \ldots$. Figure 4 shows a representative example of the time dependence of the quantum yield comparing stepladder and master equation results. As can be seen, in the present situation with near-threshold excitation, the two models do not coincide but could be brought into near coincidence by modifying the step size $|\langle\Delta E\rangle|$ of the stepladder model by roughly a factor of about 2.

Figure 5 compares the experimental[14,15] pressure dependences of the quantum yield at $\lambda = 353$ nm and $T = 220$ and 300 K with modeling results. Lennard-Jones collision frequencies have been calculated with the estimated parameters $\sigma_{LJ}(H_2CO) \approx 0.4$ nm and $\epsilon_{LJ}(H_2CO)/k \approx 400$ K (and with $\sigma_{LJ}(N_2) = 0.3798$ nm and $\epsilon_{LJ}(N_2)/k = 71.4$ K). The calculated curves sensitively depend on the precise value of the threshold energy $E_{0,1}$. In addition, they depend on the value of $\langle\Delta E\rangle$. Uncertainties in the one parameter could be compensated by changes of the other. However, the values for $\langle\Delta E\rangle$ and $E_{0,1}$ derived from the analysis of the thermal dissociation experiments in ref 7 give some orientation. Varying $\langle\Delta E\rangle$ and $E_{0,1}$ in the modeling of Figure 5 provides a second access to $E_{0,1}$. Although the master equation treatment for $E_{0,1} = 82.2$ kcal mol^{-1} gives agreement with the fairly scattered experimental quantum yields for 300 K when $-\langle\Delta E\rangle/hc = 65(\pm 15)$ cm^{-1} is chosen, similar agreement with $E_{0,1} = 81.9$ kcal mol^{-1} requires $-\langle\Delta E\rangle/hc$ to be in the range $100(\pm 20)$ cm^{-1}; see Figure 5. Agreement with the experiments for the low value $E_{0,1} = 79.2$ kcal mol^{-1} would only be obtained when $-\langle\Delta E\rangle/hc$ would be raised to values higher than 3000 cm^{-1}, which clearly can be ruled out. The analysis of pyrolysis experiments in ref 7 for $E_{0,1} = 81.7$ kcal mol^{-1} and M = Ar led to $-\langle\Delta E\rangle/hc = 100(\pm 20)$ cm^{-1} near 2500 K. As only weak temperature dependences of $\langle\Delta E\rangle$ are expected and M = N_2 and Ar often have similar values of $\langle\Delta E\rangle$, clearly only the high values of $E_{0,1}$ are consistent with the measurements of Figure 5. The present analysis, therefore, is consistent with $E_{0,1} = 81.7$ kcal mol^{-1} from the analysis of pyrolysis rate coefficients.[7] It should, however, be noted that the present analysis of photolysis requires that the same anharmonicity factors of the density of states in $k_1(E)$ are used as in the analysis of pyrolysis rate constants.[7] In both cases $F_{anh}(E{=}E_{0,1}) \approx 1.89$ was employed; see the Appendix of ref 6.

Having fixed $E_{0,1}$ and $\langle\Delta E\rangle$ by producing agreement with the experimental Stern−Volmer plot of ϕ_1 at 300 K (see Figure 5), one would expect that the experimental temperature dependence of ϕ_1 from ref 15 could also be reproduced. Unfortunately, this is not the case. Assuming temperature-independent $\langle\Delta E\rangle$ which appears most plausible, the master equation simulations predict a weaker temperature dependence of ϕ_1 than observed experimentally. One could cure this discrepancy by assuming a marked negative temperature coefficient of $\langle\Delta E\rangle$. It appears more plausible, however, to attribute the discrepancy to problems in these difficult experiments[44] and to trust more on the modeled temperature dependence of ϕ_1 (see also the discussion of experimental problems in the quantum yield measurements of ref 45).

The uncertainties and the internal inconsistency of the experiments also become evident when Stern−Volmer constants for different wavelengths are considered. The stepladder model leads to slightly curved Stern−Volmer plots at small pressures. However, the curvatures nearly disappear in the master equation treatment such as observed also earlier.[41] Therefore, linear Stern−Volmer plots of the form

$$\phi_1^{-1} = \phi_{Mol}^{-1} \approx 1 + a(\lambda,T)[M] \qquad (11)$$

appear adequate. Figure 6 compares modeled Stern−Volmer constants $a(\lambda,T)$ with the four experimental values from ref 15. It appears that the experimental wavelength dependence is approximated slightly better with $E_{0,1} = 81.9$ kcal mol^{-1} than with $E_{0,1} = 82.2$ kcal mol^{-1}. For this reason, we prefer the former value in the present work (together with the corresponding value of $-\langle\Delta E\rangle/hc = 100$ cm^{-1}). Figure 6 shows experimental inconsistencies outside the experimental error limits. We,

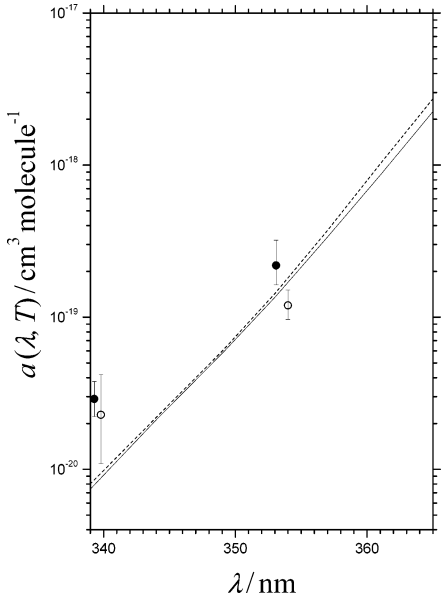

Figure 6. Stern−Volmer constants $a(\lambda,T)$ for formaldehyde photolysis on the molecular elimination channel 1: experimental results from Table 3 of ref 15 for 300 K (○) and 220 K (●). Lines: from modeling of this work with $E_{0,1} = 81.9$ kcal mol^{-1}, $-\langle\Delta E\rangle/hc = 100$ cm^{-1} in N_2 for 300 K (solid) and 220 K (dashed). See text.

therefore, suggest using the modeled Stern−Volmer constants that were fitted to a compromise between the experimental data for 300 K and the two wavelengths 339.8 and 354 nm. The modeled temperature dependence of the Stern−Volmer constants $a(\lambda,T)$ from eq 11, assuming temperature independent $\langle\Delta E\rangle$, is much smaller than the experimental uncertainty of the data from Figure 6 to which the modeling is fitted. The temperature dependence of $a(\lambda,T)$, therefore, at this stage appears negligible. The modeled $a(\lambda,300\text{ K})$ then is taken for the temperature range 200−300 K and it is approximated by

$$a(\lambda,T) \approx 5.8 \times 10^{-20} \exp[-c_a(\lambda_0-\lambda)]\ \text{cm}^3\ \text{molecule}^{-1} \quad (12)$$

with $\lambda_0 = 349$ nm; $c_a = 0.225$ nm^{-1} for $\lambda > \lambda_0$ and $c_a = 0.205$ nm^{-1} for $\lambda < \lambda_0$. This expression substantially differs from the fully empirical representations suggested in refs 4 and 13. The present recommendation is believed to have a more rational basis. However, in view of the considerable experimental uncertainty new experimental investigations appear highly desirable.

III. Quantum Yields for 310−340 nm

Unlike the range 340−360 nm, the total quantum yields for radical and molecular fragments $\phi = \phi_{Rad} + \phi_{Mol}$ in the range 310−340 nm at pressures up to 1 bar are pressure independent and close to unity.[15] Some comparably minor pressure dependences of ϕ_{Rad} have been discovered recently in the range 308−320 nm[45] (see below), but these are much smaller than the effects discussed in section II. The essentially pressure independent ϕ_{Rad} in the range 310−330 nm then does not contain information on absolute rate coefficients, such as analyzed in section II, but it is determined by ratios of specific rate constants only. We represent the corresponding branching ratio by an energy- and angular-momentum-dependent function $\phi_{Rad}(E,J)$ and relate its thermal average to the photolysis quantum yield $\phi_{Rad}(\lambda,T)$ for radical products. If channels 1−3 could be separated, $\phi_{Rad}(E,J)$ would be given by

$$\phi_{Rad}(E,J) = k_2(E,J)/[k_1(E,J) + k_2(E,J) + k_3(E,J)] \quad (13)$$

As long as the total quantum yield ϕ is close to unity, there is no need to analyze the respective contributions of channels 1 and 3 to ϕ_{Mol}, but only the partitioning of ϕ into ϕ_{Rad} and ϕ_{Mol} at $E > E_{0,2}(J)$ is required to be characterized. ϕ_{Rad} also contains some contribution from channel 4 in the tunneling range. We have modeled the rate of this channel by RRKM theory including tunneling using the approach described in section II. Like the rate of channel 2 it is not in a range where contributions to the pressure dependence of ϕ at $P < 1$ bar are expected. In addition, its contribution to ϕ_{Rad} for the present work again needs not to be separated from that of channel 2.

On the basis of classical trajectory calculations on the ab initio potential of ref 32, the energy dependence of $\phi_{Rad}(E,J)$ has been determined. It can be approximated in the form

$$\phi_{Rad}(E) \approx C_1\{1 - \exp[-[E - E_{0,2}]/C_3]\} \quad (14)$$

with $C_1 \approx 0.75$ and $C_3/hc \approx 750$ cm^{-1}. It was suggested in ref 6 that there should be an additional J dependence which was tentatively assumed to be of the type

$$\phi_{Rad}(E,J) \approx C_1\{1 - \exp[-C_2J - \{[E - E_{0,2}(J)]/C_3\}]\} \quad (15)$$

and where $E_{0,2}(J)$ denotes the J-dependent threshold energy of channel 2. From the ab initio potential $E_{0,2}(J)$ was derived to be of the form

$$E_{0,2}(J) \approx E_{0,2}(J{=}0) + C_\nu[J(J{+}1)]^\nu \quad (16)$$

with the parametes[6] $C_\nu/hc \approx 0.43$ cm^{-1} and $\nu \approx 1.0$, whereas $E_{0,2}(J{=}0)/hc = 30328.5(\pm0.5)$ cm^{-1} is known from spectroscopic measurements.[18,19] In the following we try to fit the parameter C_2 by identifying thermal averages of $\phi_{Rad}(E,J)$ with experimental quantum yields $\phi_{Rad}(\lambda,T)$ such as shown in Figures 1 and 2.

There is only negligible vibrational excitation at 300 K such that thermal averaging of $\phi_{Rad}(E,J)$ only concerns rotational excitation. To perform the thermal averaging, we approximate H_2CO by a symmetrical top with the rotational constants $A = 9.405$ cm^{-1} and $B_{eff} = (B + C)/2 = 1.2145$ cm^{-1} and assume that $E_{0,2}(J)$ does not depend on the quantum number K. $\phi_{Rad}(\lambda,T)$ then is assumed to be given by

$$\phi_{Rad}(\lambda,T) = Q_{rot.}{}^{-1}\sum_{J=0}^{\infty}(2J+1)\sum_{K=-J}^{J}\phi_{Rad}(E,J)\exp[-E_{rot.}(J,K)/kT] \quad (17)$$

with the rotational partition function $Q_{rot.}$ given by the sums over J and K putting $\phi_{Rad}(E,J) = 1$, $\phi_{Rad}(E,J)$ from eq 15 with $E = hc/\lambda + E_{rot.}(J,K)/hc$ and $E_{rot.}(J,K) = B_{eff}J(J{+}1) + (A - B_{eff})K^2$. Figure 7 compares the results from eq 17 with the experimental $\phi_{Rad}(\lambda,300\text{ K})$, varying the parameters C_2 and C_3. The influence of C_3 is only minor in comparison to that of C_2. However, even the latter influence is not too pronounced and a calculation with $C_2 = 0$ is not too far from the experimental results. Nevertheless, optimum agreement with the data from refs 14−17 seems to be achieved with $C_2 = 0.05$. This value is higher than the value $C_2 = 0.003$ fitted to thermal branching ratios,[7] which practically corresponds to the curve with $C_2 = 0$ in Figure 7. One may argue about whether the difference is significant or not. If the effect would be real, it could be attributed to slightly different initial distributions of the dissociative trajectories created by thermal (collisional) and optical

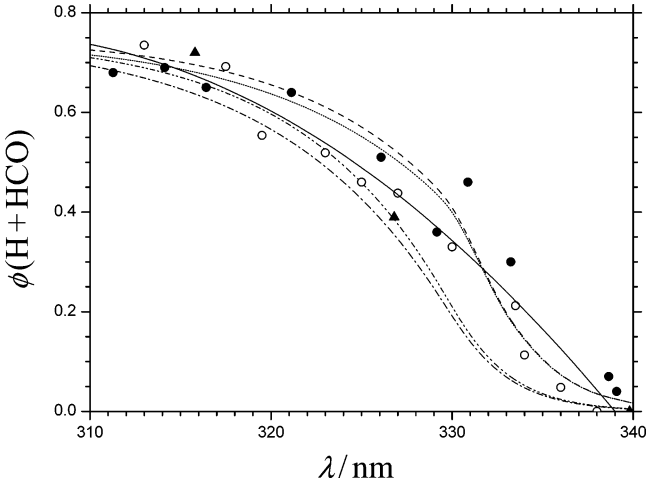

Figure 7. Quantum yields of formaldehyde photolysis to radical products. For experimental results (symbols and solid line), see Figure 1. Modeling by eqs 15−17 with $C_1 = 0.75$ and (C_2, C_3)/hc (cm^{-1}) = (0, 750) (-···-), (0, 850) (·-·), (0.05, 750) (---), and (0.05, 850) (···). See text.

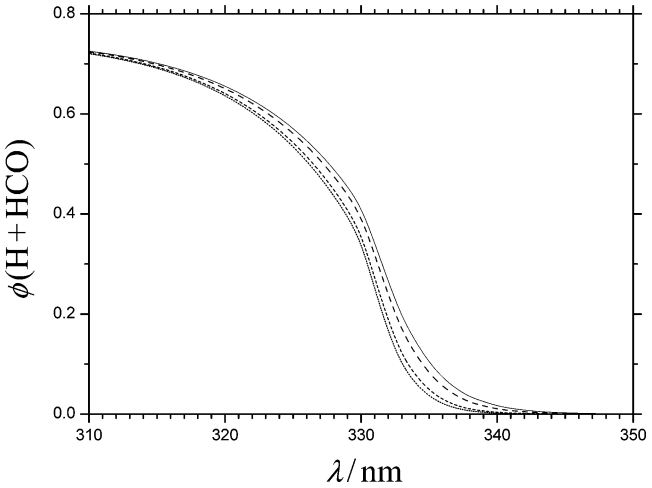

Figure 8. Modeled temperature dependence of quantum yields of formaldehyde photolysis to radical products. Curves from bottom to top: T/K = 200, 220, 270, and 300. Modeling by eqs 15−17 with $C_1 = 0.75$, $C_2 = 0.05$, and C_3/hc = 750 cm^{-1}. See text.

excitation (absorption followed internal conversion). One also might think about similar phenomena to be responsible for the minor pressure dependences of $\phi_{Rad}(\lambda,T)$ observed in ref 45 in the range 308−320 nm. Collisions here might modify the starting conditions of the dissociation dynamics after the individual excitations (configurations, angular momenta) and, hence, influence the finer details of ϕ_{Rad} (λ,T). Pressure effects arising from the contribution of channel 4 to radical formation in the tunneling range of this channel appear much less probable.

Equation 15 contains two dependences of $\phi_{Rad}(E,J)$ on J, one through the factor C_2 and one through the J dependence of $E_{0,2}(J)$. The major part of the temperature dependence of $\phi_{Rad}(\lambda,T)$ is due to the latter. Fixing $C_2 = 0.05$ and employing $E_{0,2}(J)$ from eq 16, the modeled temperature dependence of $\phi_{Rad}(\lambda,T)$ from the thermally average of eq 17 is illustrated in Figure 8. One observes that not only the range $\lambda > 329.7$ nm $= hc/E_{0,2}(J=0)$ is affected by thermal excitation but also, to a minor extent, the range $\lambda < 329.7$ nm, which is due to the presence of the two components of the J dependence of $\phi_{Rad}(E,J)$.

In view of the qualitative agreement between modeled and experimental quantum yields $\phi_{Rad}(\lambda.300\ K)$, one can represent the results from Figures 7 and 8 in analytical form. Equation 18 gives the results

$$\phi_{Rad}(\lambda,T) \approx C_1\{1 - \exp[-(\lambda_0^{-1} + 3kT/hc - \lambda^{-1})/(C_3/hc)]\} \quad (18)$$

for $\lambda \le \lambda_0$ with $C_1 \approx 0.75$, $C_3/hc = 750\ cm^{-1}$, and $\lambda_0 = 329.7$ nm and

$$\phi_{Rad}(\lambda,T) \approx \phi_{Rad}(\lambda_0,T)\exp[-(\lambda_0^{-1} - \lambda^{-1})2hc/3kT] \quad (19)$$

for $\lambda > \lambda_0$ with $\phi_{Rad}(\lambda_0,T)$ given by eq 18. The present modeling cannot decide which of the scattered experimental points at $\lambda > 330$ nm are the best, because, apart from $E_{0,2}(J)$, the parameter C_2 has to be fitted to the experiments. In addition, the modeling function of eq 15 is still in a preliminary state. Hopefully, future more detailed trajectory calculations of the E and J dependence of $\phi_{Rad}(E,J)$, therefore, will be helpful.

IV. Conclusions

The present modeling of the quantum yields of formaldehyde photolysis to radical and molecular products has demonstrated that the experimental results within the experimental accuracy are consistent with thermal dissociation rate coefficients and with theoretical branching ratios and rate coefficients calculated on the ab initio potential. Refinements on all levels of this comparison are desirable. Nevertheless, the basic consistency appears to be well established and the given approximate analytical representation of the quantum yields as functions of pressure, temperature, and wavelength allow one to extrapolate into experimentally not easily accessible ranges.

Acknowledgment. I acknowledge many stimulating discussions with James A. Miller. I thank S. D. Chambreau and Joel Bowman for a preprint of ref 26 and A. I. Maergoiz for technical assistance. Financial support of the Deutsche Forschungsgemeinschaft (SFB 357 "Molekulare Mechanismen unimolekularer Prozesse") is also gratefully acknowledged.

References and Notes

(1) Meller, R.; Moortgat, G. K. *J. Geophys. Res.* **2000**, *105*, 7089.
(2) Miller, J. A.; Pilling, M. J.; Troe, J. *Proc. Combust. Inst.* **2005**, *30*, 43.
(3) Baulch, D. L.; Bowman, C. T.; Cobos, C. J.; Cox, R. A.; Just, Th.; Kerr, J. A.; Pilling, M. J.; Stocker, D.; Troe, J.; Tsang, W.; Walker, R. W.; Warnatz, J. *J. Phys. Chem. Ref. Data* **2005**, *34*, 757.
(4) Sander, S. P.; Friedl, R. R.; Golden, D. M.; Kurylo, M. J.; Huie, R. E.; Moortgat, G. K.; Keller-Rudek, H.; Wine, P. H.; Ravishankara, A. R.; Kolb, C. E.; Molina, M. J.; Finlayson-Pitts, B. J.; Orking, V. L. *NASA-JPL Evaluation No. 15*, **2006**, *JPL Publication 06−2*.
(5) Atkinson, R.; Baulch, D. L.; Cox, R. A.; Crowley, J. N.; Hampson, R. F.; Hynes, R. G.; Jenkin, M. E.; Rossi, M. J.; Troe, J. *Atmos. Chem. Phys.* **2006**, *6*, 000.
(6) Troe, J. *J. Phys. Chem. A* **2005**, *109*, 8320.
(7) Troe, J. *J. Phys. Chem. A* **2007**, *111*, 3862.
(8) Green, W. H.; Moore, C. B.; Polik, W. F. *Annu. Rev. Phys. Chem.* **1992**, *43*, 591.
(9) Chuang, M.-C.; Foltz, M. F.; Moore, C. B. *J. Chem. Phys.* **1987**, *87*, 3855.
(10) Yamaguchi, Y.; Wesolowski, S. S.; Van, Huis, T. J.; Schaefer, H. F., III. *J. Chem. Phys.* **1998**, *108*, 5281.
(11) Valachovic, L. R.; Tuchler, M F.; Dulligan, M.; Droz-Georget, Th.; Zyrianov, M.; Kolessov, A.; Reisler, H.; Wittig, C. *J. Chem. Phys.* **2000**, *112*, 2752.
(12) Bowman, J. M.; Zhang, X. *Phys. Chem. Chem. Phys.* **2006**, *8*, 321.
(13) Calvert, J. G.; Atkinson, R.; Kerr, R. A.; Madronich, S.; Moortgat, G. K.; Wallington, T. J.; Yarwood, G. *The Mechanism of Atmospheric Oxidation of the Alkenes*; Oxford University Press: New York, Oxford, 2000.
(14) Moortgat, G. K.; Warneck, P. *J. Chem. Phys.* **1979**, *70*, 3639.

(15) Moortgat, G. K.; Seiler, W.; Warneck, P. *J. Chem. Phys.* **1983**, *78*, 1185.
(16) Horowitz, A.; Calvert, J. C. *Int. J. Chem. Kinet.* **1978**, *10*, 805.
(17) Smith, G. D.; Molina, L. T.; Molina, M. J. *J. Phys. Chem. A* **2002**, *106*, 1233.
(18) Terentis, A. C.; Kable, S. H. *Chem. Phys. Lett.* **1996**, *258*, 626.
(19) Terentis, A. C.; Waugh, S. E.; Metha, G. F.; Kable, S. H. *J. Chem. Phys.* **1998**, *108*, 3187.
(20) Feller, D.; Dupuis, M.; Garrett, B. C. *J. Chem. Phys.* **2000**, *113*, 218.
(21) Townsend, D.; Lahankar, S. A.; Lee, S. K.; Chambreau, S. D.; Suits, A. G.; Zhang, X.; Rheinecker, J.; Harding, L. B.; Bowman, J. M. *Science* **2004**, *306*, 1158.
(22) Zhang, X.; Rheinecker, J. L.; Bowman, J. M. *J. Chem. Phys.* **2005**, *122*, 114313.
(23) Yin, H.-M.; Nauta, K.; Kable, S. H. *J. Chem. Phys.* **2005**, *122*, 194312.
(24) Chambreau, S. D.; Lahankar, S. A.; Suits, A. G. *J. Chem. Phys.* **2006**, *125*, 044302.
(25) Lahankar, S. A.; Chambreau, S. D.; Townsend, D.; Suits, F.; Farnum, J.; Zhang, X.; Bowman, J. M.; Suits, A. G. *J. Chem. Phys.* **2006**, *125*, 044303.
(26) Lahankar, S. A.; Chambreau, S. D.; Zhang, X.; Bowman, J. M.; Suits, A. G. *J. Chem. Phys.* **2006**, submitted.
(27) Forst, W. *J. Phys. Chem.* **1983**, *87*, 4489.
(28) Troe, J. *J. Phys. Chem.* **1984**, *88*, 4375.
(29) Bauerfeldt, G. F.; de Albuquerque, L. M. M.; Arbilla, G.; Da, Silva, E. C. *J. Mol. Struct. (THEOCHEM)* **2002**, *580*, 147.
(30) Atkinson, R.; Baulch, D. L.; Cox, R. A.; Hampson, R. F.; Kerr, R. A.; Troe, J. *J. Phys. Chem. Ref. Data* **1989**, *18*, 881.
(31) Van, Zee, R. D.; Foltz, M. F.; Moore, C. B. *J. Chem. Phys.* **1993**, *99*, 1664.
(32) Zhang, X.; Zou, S.; Harding, L. B.; Bowman, J. M. *J. Phys. Chem. A* **2004**, *108*, 8980.
(33) Polik, W. F.; Guyer, D. R.; Moore, C. B. *J. Chem. Phys.* **1990**, *92*, 3453.
(34) Goddard, J. D.; Schaefer, H. F., III. *J. Chem. Phys.* **1979**, *70*, 5117.
(35) Clouthier, D. J.; Ramsay, D. A. *Annu. Rev. Phys. Chem.* **1983**, *34*, 31.
(36) Miller, W. H. *J. Am. Chem. Soc.* **1979**, *101*, 6810.
(37) Kato, S.; Morokuma, K. *J. Chem. Phys.* **1980**, *72*, 206.
(38) Yonehara, T.; Kato, S. *J. Chem. Phys.* **2002**, *117*, 11131.
(39) Yonehara, T.; Kato, S. *J. Chem. Phys.* **2006**, *125*, 084307.
(40) Moore, C. B.; Weisshaar, J. C. *Annu. Rev. Phys. Chem.* **1983**, *34*, 525.
(41) Troe, J. *J. Phys. Chem.* **1983**, *87*, 1800.
(42) Baggott, J. E. *Chem. Phys. Lett.* **1985**, *119*, 47.
(43) Troe, J. *J. Chem. Phys.* **1977**, *66*, 4745.
(44) Moortgat, G. K. Private communication, 2006.
(45) Pope, F. D.; Smith, C. A.; Davis, P. R.; Shallcross, D. E.; Ashfold, M. N. R.; Orr-Ewing, A. J. *Faraday Discuss. Chem. Soc.* **2005**, *130*, 59.